

New insights into the catastrophic slope failures at Sau Mau Ping: the role of antecedent rainfall pattern



Abstract Climate change is increasing the frequency and intensity of extreme rainfall events, which aggravate the threat to the safety of natural and man-made slopes. There is growing interest in the role of rainfall characteristics in these slope failures. Most of previous studies treated the rainfall individually or as cumulative value and used hypothetical rainfall temporal patterns with no association with actual physical failures. In this study, the two deadly landslides in Sau Mau Ping, Hong Kong, in June 1972 and August 1976, which caused 165 casualties, are revisited. An intriguing question that has long been overlooked is posed: *why the slopes that withstood the 1972 rainfall failed in the 1976 rainfall, given that the rainfall intensity of the latter event was only half of the former?* Based on an extensive review of the forensic reports and relevant studies on the failure events, numerical modeling is carried out by a combination of seepage analysis with stability analysis and unsaturated shear strength theory. Focus is placed on the geological and hydrological settings and the rainfall characteristics, particularly the temporal pattern of the antecedent and main rainfall, to look into the causes and mechanisms for these failures. Implications of the new findings for future research and practice are also highlighted.

Keywords Rainfall-induced landslides · Antecedent rainfall · Rainfall temporal pattern · Landslide hazard

Introduction

Rainfall-induced slope failures are among the most devastating and alarming natural disasters, as demonstrated by, for example, the 1999 Venezuela landslide and flood disaster, which resulted in a catastrophic death toll of over 15,000 (Iverson 2000) and the 2009 Hsiaolin (Taiwan) landslide which killed more than 400 people (Yang et al. 2018). Numerous studies from different perspectives, including geotechnical, climatological, and hydrological, have been conducted to understand the underlying mechanisms. These studies utilized laboratory experiments (Yang 2002; Ng et al. 2004; Yang and Wei 2012), physical models (Eckersley 1990; Wang and Sassa 2001; Take et al. 2004; Ng et al. 2022), field instrumentations (Li et al. 2005; Godt et al. 2009; Springman et al. 2013), numerical models (Cascini et al. 2010, 2013), and theoretical studies (Iverson 2000; Godt et al. 2012). Results and views found in the literature are divergent, indicating the complexity of interplays of various factors (Wang and Sassa 2001; Guzzetti et al. 2007; Zhang et al. 2011; Natalia and Yang 2022).

On the basis of the effective stress theory in soil mechanics, rainfall-induced failure is often seen as the result of the saturation process of the soil, which can gradually weaken the slope. Also, it

has been well accepted that the in situ state of soil (i.e., density and confining pressure) are two key factors controlling the mechanical behavior of soil under external loading conditions. Loose soil contracts and dense soil dilates, subsequently causing the strain-softening and strain-hardening behavior, respectively. Several studies highlighted the critical roles of fines and grain shape in causing flow liquefaction of sandy soils (Yang and Wei 2012; Wang and Sassa 2003) and the influence of the static driving shear stress on the onset of the flow failure (Yang et al. 2021). The flume experiments of Wang and Sassa (2001) showed that there is an optimum density which facilitates the pore pressure build-up and slope failure.

Precipitation is often considered as the main trigger for rainfall-induced slope failures. The soil permeability controls the ease and difficulty of water flowing in and out of the soil mass. When the permeability is low, the desaturation process requires a longer duration compared to high-permeability soil. Hence, the soil retains more water within its voids under the same duration. When water infiltrates the soil, it conducts more freely within the soil mass and can be easily redistributed. A common assumption used in analyzing the infiltration process is that the maximum infiltration rate to a soil body equals the saturated permeability of the soil (Zhang et al. 2011). However, field instrumentation (Li et al. 2005) and numerical model (Gasmo et al. 2000) show that it may not always be the case.

Some studies are interested in identifying the threshold conditions of slope failures from the perspective of rainfall characteristics, such as intensity, duration, and frequency (Rahardjo et al. 2007; Zhang et al. 2011; Yubonchit et al. 2017), which are useful for developing variations of intensity-duration (ID curve) and early-warning systems (Chen et al. 2017; Gao et al. 2018; Kong et al. 2020; Lee et al. 2021; Zhao et al. 2022). Springman et al. (2013) conducted field monitoring of a shallow weathered slope in Switzerland to study the bi-seasonal response of the slope stability. Take et al. (2015) utilized geotechnical centrifuge modeling to quantitatively evaluate the effect of different antecedent conditions on landslide mobility and hazards. Both studies indicated that the landslide mechanisms depend on the saturation state of the soil mass and the rainfall history. The implication is that the antecedent conditions need to be examined when considering the rainfall ID thresholds.

The above discussion suggests that particular soil states and rainfall phenomena are the necessary and triggering conditions of slope failures, respectively. However, despite having similar soil characteristics, not all slopes would fail under a similar rainfall event. Likewise, despite being “loose enough,” the model slope in the physical experiment of Take et al. (2004) did not fail under the expected failure mechanism under the assigned rainfall.

There should exist some facilitating conditions that aid the rate of strength reduction and increase failure occurrence (Johnson and Sitar 1990; Anderson and Sitar 1995; Johnston et al. 2021; Natalia and Yang 2022). The presence of hydrological characteristics such as constrictive conductive zones and preferential drainage paths facilitates localized pore water development and soil strength reduction. Moreover, geological structures such as cracks and ground fissures can further facilitate drainage paths and seepage formation (Napolitano et al. 2016). Geotechnical features such as slope height, inclination angle, groundwater table, and soil parameters control the initial slope stability and the subsequent failure potential (Chiu et al. 2012; Yubonchit et al. 2017). Ng (2008) presented a comprehensive review of centrifuge tests that utilized different means to trigger destabilization (e.g., artificial rainfall infiltration, rising groundwater, downward seepage flow, and dynamic loading) to understand the failure mechanisms of loose and dense soil. A similar conclusion was found that a strain-softening material is not sufficient to induce liquefaction flowslides. An additional trigger, such as a certain seepage condition, is necessary. Additionally, Hong et al. (2018) studied the effect of inter-(rainfall) event time definitions of 231 landslide histories in South Korea and concluded that the ID threshold differed depending on inter-event durations. Similarly, Ibsen and Casagli (2004) utilized nearly a century dataset of landslides in Italy and found that landslide incidence generally follows the periodic pattern of precipitation with a particular lag duration. They postulated that the lag is related to the time necessary for the ground to develop a critical groundwater level to initiate slope failures.

In recent years, advances in understanding infiltration mechanisms have brought interest in evaluating the contribution of antecedent conditions and spatiotemporal patterns of rainfall towards landslide hazards (Parsons and Stone 2006; Mathew et al. 2014; Harilal et al. 2019; Jones et al. 2021). Rahardjo et al. (2008) conducted field instrumentation and concluded that 5-day antecedent rainfall could affect slope stability in Singapore. While studies have been conducted to identify the critical duration of the antecedent rainfall, the conclusions are still divergent, ranging from 24 h to 35 days (Guzzetti et al. 2008; Smolíková et al. 2016; Chitu et al. 2017; Harilal et al. 2019; Kong et al. 2020; Kim et al. 2021). Most of these studies account for the effect of antecedent rainfall as cumulative rainfall values or rolling rainfall amounts. Rahimi et al. (2011) compared the stability response of a homogeneous slope under various antecedent rainfall patterns including advanced, normal, and delayed rainfall patterns. Similarly, Fan et al. (2020) studied the role of rainfall temporal patterns resembling the bell-curved distribution with various kurtosis and skewness values to represent the rainfall intensity and temporal distribution, respectively. Both studies concluded that the rainfall temporal pattern influences the simulated infiltration and subsequently affects the timing and volume of rainfall-induced failures. For a similar total rainfall intensity and duration, the uniform-rainfall intensity events are found to promote failure relative to the bell-curved rainfall patterns with extreme intensity. Most of these studies are based mainly on hypothetical and relatively simplified rainfall patterns that are not associated with *actual* physical failures.

Rainfall-induced slope failures have been a major concern in Hong Kong since the 1970s. Due to the rapid increase in land demand in the 1970s, a hurried formation of embankments was

carried out by end-tipping in many places of Hong Kong, including the Sau Mau Ping area (Fig. 1). On June 18, 1972, after an extreme rainfall event with a maximum intensity of 98.7 mm/h, the slope SMP72 failed, releasing 4000 m³ of soil mass and causing 123 casualties. Following the failure, the slopes in the nearby areas were inspected, including the SMP6 slope. The SMP6 was classified as “reasonably safe” with minor works such as clearing the blocked drains and removing rubbish from the slope recommended in the evaluation. Nonetheless, four years later, in 1976, four embankment slopes that had successfully survived the 1972 extreme rainfall, including SMP6, failed, releasing 2000 m³ of soil mass and causing 42 casualties. However, the maximum rainfall intensity was only 51.5 mm/h, nearly half of the 1972 rainfall intensity.

The catastrophic failures at Sau Mau Ping raised concerns about the city-wide slope engineering practice and motivated studies by researchers and practitioners to provide explanations for the distressing events. The earliest forensic study (Yang et al. 1972; Binnie and Partners 1976) concluded that both the 1972 and 1976 events were triggered by water infiltration associated with extreme rainfalls (Vail 1984; Malone 1988). Furthermore, Sun (1999) utilized the finite difference method to simulate the 1976 slope failure, concluding that the high velocity and enormous runaway distance of the soil mass were attributed to the strain-softening behavior of the loose fill. The mechanical behavior of the local soils, such as decomposed granite and volcanic, have been studied by means of laboratory experiments. Compared with the volcanic soils, the decomposed granite, which was used as fill material to construct the slopes, is widely considered to have higher liquefaction potential (HKIE 2003; Ng et al. 2004). The effect of uncertainty in soil strength and hydraulic parameters of the 1976 slope failure was also studied (Zhang et al. 2016). While most studies in the literature focused solely on the 1976 failure event, there is an intriguing question that has long been overlooked: *Why the slopes that withstood the extreme rainfall in 1972 failed in the 1976 rainfall event, given that the latter had a much lesser maximum intensity?* This study attempts to address this question by collectively considering various factors involved. The new hypothesis proposed here is that the rainfall patterns, particularly the antecedent conditions, played a critical role in the occurrence of the two failures at Sau Mau Ping. Whether this hypothesis stands to explain the phenomenon is explored in this study.

Compared with idealized model slopes, real case histories of slope failures can serve as a valuable reference for investigating the complex interactions of geological, hydrological, and climatological settings. The Sau Mau Ping failure cases are unique in that multiple extreme rainfalls with different antecedents, and main rainfall patterns were involved. To the author’s best knowledge, the role of the temporal pattern of antecedent rainfall towards slope stability has not yet been discussed with reference to an actual physical failure in conjunction with real rainfall data, at least to the scale of Sau Mau Ping landslides. In this paper, an extensive review of the failure events is presented first. Then, numerical modeling of the hydrological and mechanical responses of the SMP72 and SMP6 slopes for three recorded rainfall events of 1966, 1972, and 1976 is described. The responses are examined and compared against the recorded data to validate the modeling. The study reveals the critical role of rainfall patterns, specifically the antecedent rainfall conditions, and its interplays with the geological and hydrological settings of the slopes.

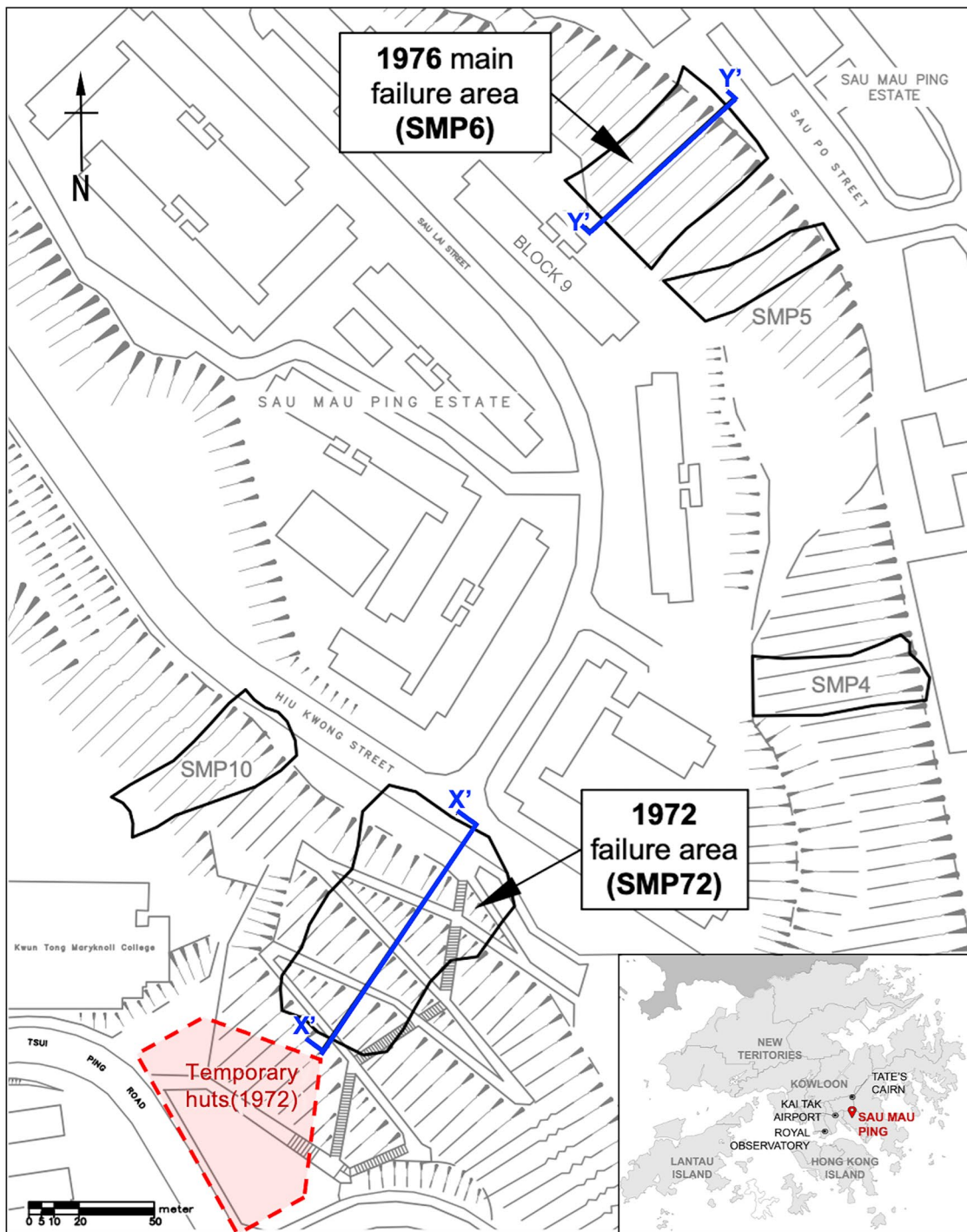


Fig. 1 Sau Mau Ping 1972 and 1976 landslide area

Numerical modeling strategy

Rainfall-induced slope failures are often associated with the downward water flux introduced by precipitation. In reality, soil near the surface is rarely under saturated conditions. This means the void between the soil grains is partially filled with air, hence, the term unsaturated. When unsaturated slopes are subjected to rainfall, the infiltration process causes changes in the water content

and consequently changes in pore water pressure. This will lead to stress state changes and soil deformation and, subsequently, affect the seepage behavior. Due to the complex nature of soil behavior under rainfall, numerical modeling is often used to study the slope failure associated with rainfall. When properly designed, numerical modeling allows a broader range of observations compared to the field measurements, especially in terms of time scale, and allows a

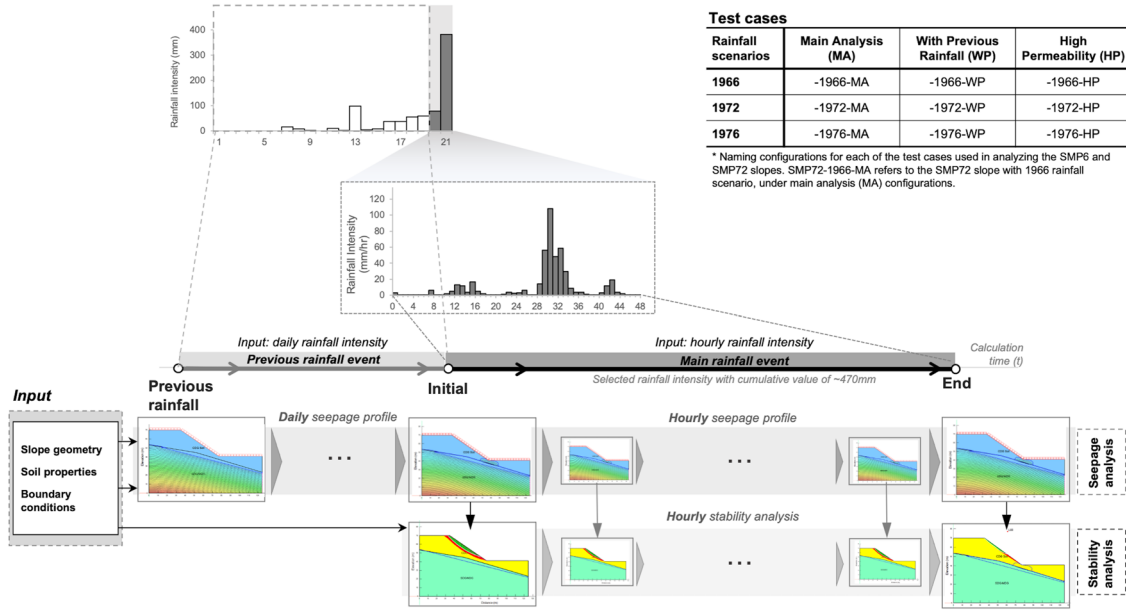


Fig. 2 Schematics of the methodology proposed in this study

detailed parametric study. It is beneficial for forensic analysis—and can be validated against well-documented events.

Figure 2 presents the methodology for each analysis in this study. For each time increment, a two-step analysis is performed. First, a seepage analysis of the slope is performed to model the respective rainfall intensity. The pore water pressure obtained from the seepage analysis is then used as an input to the stability analysis to calculate the safety factor, FOS, of the

slope at the time. The pore water pressure is also used as an input for the subsequent seepage calculation. The process is repeated for each time increment. For the “main rainfall event,” which refers to the recorded rainfall that led to the failure event, hourly time increments are selected to match the actual rainfall records (Fig. 3d–f). In this study, the two-dimensional transient water flow theory (Fredlund et al. 2012), as defined below, is utilized to study transient water pressure resulting from the applied rainfall.

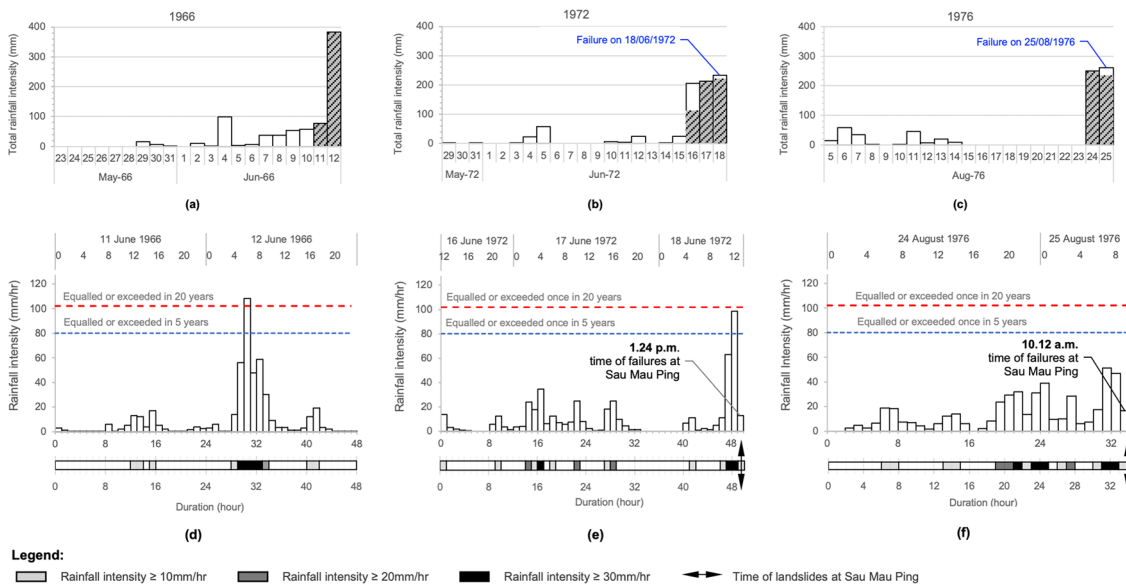


Fig. 3 Previous 19-days rainfall in a 1966, b 1972, and c 1976. Main rainfall loading in d 1966, e 1972, and f 1976, values are selected such that the cumulative intensity is approximately 470 mm

$$m_w^2 \gamma_w \frac{\partial h_t}{\partial t} = \frac{\partial}{\partial x} \left(-k_{wx} \frac{\partial h_t}{\partial x} \right) + \frac{\partial}{\partial y} \left(-k_{wy} \frac{\partial h_t}{\partial y} \right) + q \quad (1)$$

where m_w^2 , γ_w , h_t , t , k_{wx} , k_{wy} , and q are the slope of the soil water-characteristic curve, unit weight of water, total head, elapsed time, coefficients of permeability corresponding to the volumetric water content in x -direction and y -direction, and the applied (rainfall) flux, respectively. Equation 1 is solved using the well-accepted computer program SEEP/W (GeoSlope 2018).

To account for the effect of infiltration on slope stability, a shear strength model that incorporates the contribution from suction is needed. In this study, the non-linear unsaturated shear strength model of Vanapalli et al. (1996) is used. The equation is defined as follows:

$$\tau = c' + (\sigma_n - u_a) \tan \phi' + (u_a - u_w) \left[S_e \tan \phi' \right] \quad (2)$$

where τ , c' , σ_n , u_a , u_w , and ϕ' are the shear strength, effective cohesion, total normal stress, pore air pressure, pore water pressure, and friction angle, respectively. The $(\sigma_n - u_a)$ and $(u_a - u_w)$ correspond to net normal stress on the failure plane and matric suction, respectively. Thus, the first, second, and third components in Eq. 2 account for the contribution of cohesive, frictional, and suction strength to the soil, respectively. The effective degree of saturation S_e is responsible for quantifying the non-linear contribution of the suction to the shear strength, which is defined as:

$$S_e = \left(\frac{\theta_w - \theta_r}{\theta_s - \theta_r} \right) \quad (3)$$

where θ is the volumetric water content, and the subscripts w , r , and s indicate the current, residual, and saturated conditions, respectively.

The non-linear strength definition provides a more realistic representation of unsaturated behavior. Generally, the shear strength of unsaturated soil increases with matric suction until the air-entry value is reached. At a higher magnitude of suction, the suction strength decreases non-linearly in proportion to the effective degree of saturation. When the field volumetric water content is equal to the residual value, the contribution of suction to the shear strength is equal to zero.

The slope stability analysis is performed using the Morgenstern-Price method implemented in SLOPE/W (GeoSlope 2018). The strength Eq. 2 is input to account for the stability of the unsaturated slope under rainfall conditions.

Case study: Sau Mau Ping slope failures

This section gives a brief summary of the Sau Mau Ping slope failures. The bedrock in the Sau Mau Ping area is formed by granite, one of the two dominant rock types in Hong Kong besides volcanic rock. These rocks are deeply weathered in situ, with highly variable weathering depth, reaching up to 60 m. The site, located between elevations 45 and 90 mPD, covered five main tributaries that drained southwestwards to a stream draining southeastwards near Hip Wo Street and Tsui Ping Road, shown in Fig. 1. After the construction, the drainage pattern was modified by providing catchwater and stormwater drains. The valleys of the tributaries were filled as part of the platform using decomposed granite taken from adjoining site formation, part of which became SMP72 and SMP6, the failure area in 1972 and 1976, respectively.

The site formation was completed between 1964 and 1965. However, some of these slopes had a history of instability, even during the time of the site formation works. Most of these failures were relatively small scale, such as erosion and shallow slides, none of which caused casualties. Binnie and Partners (1976) recorded erosion and surface slides that were visible to the slope areas, including the SMP5, 6, 10, and 72 after the 1966 extreme rainfall. The original slope protection measures were proven inadequate as multiple instabilities kept occurring between 1965 and 1968. Several remedial works were commenced within that period, focusing on erosion prevention, such as providing stone pitching on the lower half sections, construction of additional drainage systems, and turfing over the upper half of the slope surface.

The slope SMP72, located between Hiu Kwong Street and Tsui Ping Road, failed on June 18, 1972, at 1.24 p.m. The failure was preceded by a series of extreme rainfall with a total rainfall of 650 mm, which started on June 16, 1972 (Fig. 3b, e). The maximum rainfall intensity of 98.7 mm/h was recorded around 1 h before the failure commenced. The failure was located right on top of the Sau Mau Ping Class II Licensed Area, a resettlement area proposed by the local government in 1964, which consisted of temporary huts to accommodate homeless refugees (see areas bounded by red-dotted lines in Fig. 1). The area was engulfed by the fallen earth and rocks almost immediately after the ground movement was noticed, causing 71 fatalities and injured 60 others.

The extreme rainfall occurring on 16–18th of June 1972 also caused another deadly landslide on the same day at Po Shan Road, causing 67 fatalities, 20 injuries, and the failure of three buildings. The failure mechanisms of the 1972 Po Shan Road and Sau Mau Ping failures were assumed to be similar at that time, although several studies suggested different views (Yang et al. 2008; Luo et al. 2021). Thus, the Po Shan Road incident was widely selected as the study case in the literature. There are no quantitative attempts to study the Sau Mau Ping 1972 failure prior to this study.

Four years after the deadly landslides, on August 25, 1976, at 10.12 a.m., another disastrous failure happened in the Sau Mau Ping area. The failures were recorded at four locations, two at SMP6, one at SMP5, and another at SMP10 (Fig. 1). *What is intriguing is that all these slopes were examined right after the 1972 failures and were considered reasonably safe.* Remedial works following the suggestions of the inspectors also followed the examinations. In this study, we focus on the main failure site at SMP6, which formed a flowslide and impinged on Block 9 of the estate, inundating the ground floor, killing 18 people, and causing serious injuries to 24 others. Figure 3c, f shows the rainfall intensity prior to the failures.

Modeling setup and parameter selection

The slope profiles used for numerical modeling of SMP72 and SMP6 are shown in Fig. 4a and b, respectively, which are determined by referring to the available topography and water courses map, construction schedule of the slopes, drillholes, trial pits, and piezometer readings from the forensic reports (Binnie and Partners 1976; Knull et al. 1999; Vail 1984; Yang et al. 1972). These profiles are taken from cross-sections $X'-X'$ and $Y'-Y'$ in Fig. 1 (blue lines), which were located at the main failure area of SMP72 and SMP6, respectively. The slopes were comprised of CDG (completely decomposed granite) fill overlaying the MDG/SDG (moderately/

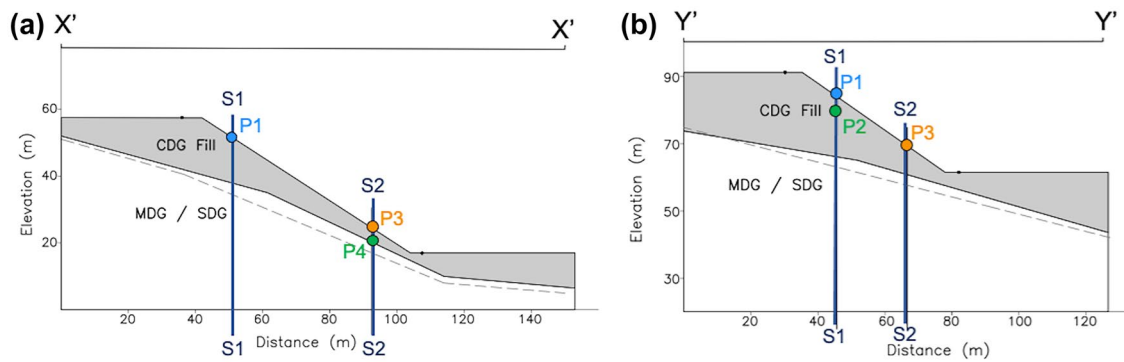


Fig. 4 Slope cross-sections of **a** SMP72 and **b** SMP6

slightly decomposed granite) bedrock. The inclination angle of SMP72 and SMP6 is taken as 32.83° and 34.62° , respectively. The groundwater table is approximated from the piezometer readings shown in Fig. 4a, b as dotted lines. The pore water is set to be hydrostatic with a maximum suction of 10 kPa, based on field measurements of Li (2003). Two cross-sections, S1 and S2, located 10 m from the slope's crest and toe, are drawn to observe the pore water development due to the rainfall. Four flux points are selected to observe the seepage and infiltration characteristics. Points P1 and P3 are located on the slope surface on the top of the S1 and S2 cross-sections, respectively. Points P2 and P4 are located at the depth of the critical slip of SMP6 and SMP72, respectively.

Table 1 shows the parameters used for the seepage and stability analysis. These parameters are determined based on a careful study of the forensic reports and relevant studies on Sau Mau Ping failures (Binnie and Partners 1976; Vail 1984; Sun 1999; Zhang et al. 2016), and they are representative of the materials involved. As the variability of unit weight is relatively small, a typical value (18 kN/m^3) is used for simplicity. For strength parameters, a variation with depth is assumed (Sweeney and Robertson 1979) to reflect field conditions (inhomogeneity and

spatial variability) and the potential influence of slope construction method (end tipping), since the thickness of the fill is rather large. The permeability coefficients were measured from boreholes using the constant head method, and the average saturated permeability is used for the CDG fill. For the high permeability (HP) cases, one magnitude higher is assigned to the CDG fill to study the possibility of uncertainty in terms of permeability in explaining the 1976 failure. The SWCC of the soil is taken from the study on other similar slopes by Jiao et al. (2005) as there was no direct measurement for SWCC of CDG fill and MDG/SDG at Sau Mau Ping.

–Three sets of rainfall data, 1966, 1972, and 1976 rainfall events, are modeled in this study. The 1966 rainfall is included here because it had an extreme rainfall intensity of 108 mm/h , more significant than that in the 1972 and 1976 rainfall events, but only minor failures were recorded. Thus, we would like to investigate the differences between these rainfall events and how they affected the slope stability. All these rainfall cases are applied as flux sections on the slope surface to simulate the infiltration process.

The rainfall datasets have been obtained from different references. Three measurement gauges (Fig. 1) located near the

Table 1 Summary of the input parameters used in the modeling

Input parameters			CDG fill	MDG/SDG
Seepage analysis	SWCC [(Fredlund and Xing 1994) equation]	θ_s	0.37	0.08
		a_f	1.70	0.20
		n_f	2.10	5.00
		m_f	0.30	0.45
		Permeability (m/s) [(Fredlund et al. 1994) approximation]	k_{sat}	2.68×10^{-6} (2.68×10^{-5}) ^b
Slope stability	Unit weight (kN/m^3)	γ_{sat}	18	18
	Friction angle ^a	ϕ'	$34^\circ - 36.8^\circ$	45°
	Cohesion (kPa) ^a	c'	0 – 2	10

^aThe friction angle and cohesion of CDG fill is set to be increasing with depth with direction parallel to the slope's surface

^bPermeability coefficient used in high permeability (HP) cases

site provided hourly rainfall records prior to these failures: Tate's Cairn, Kai Tak Airport, and Royal Observatory (Binnie and Partners 1976; Royal Observatory 1977, 1979). However, only daily measurement readings measured at Royal Observatory are available for the “previous rainfall event” analysis (Hong Kong Observatory 2023). Thus, for consistency purposes, the rainfall data recorded at Royal Observatory are used in this study. Rainfall intensity is defined as the total amount of rain falling for a given period of interest (duration). The duration is the length of time of the rainfall. In this study, the hourly rainfall record is used to evaluate the influence of rainfall temporal pattern towards seepage and slope stability. Additionally, daily rainfall data records are also used to establish the “previous rainfall” which is used to evaluate the antecedent condition.

The “previous rainfall event” in this study (Fig. 2) refers to the 19-day rainfall prior to the recorded extreme rainfall. When no “previous rainfall event” is applied, the slope’s initial condition depends on the input parameters, and the calculation steps are the “initial to the end” steps in Fig. 2. The slopes have identical initial seepage. It is particularly useful to isolate the effect of the “main rainfall event” on the seepage and slope stability as in “Main Analysis” (MA) test cases. The “main rainfall event” is selected to have a cumulative rainfall intensity of approximately 470 mm based on considerations of the rainfall intensity and duration of the extreme rainfall events leading to the failure and the data availability. The previous and main rainfall events are represented as white and grey shaded bars, respectively, in Fig. 3a–c. The hourly rainfall patterns, which are used as input for the main rainfall events, are shown in Fig. 3d–f. The forensic reports have recorded substantial variability on the failure sites. Thus, another set of test cases with higher permeability input for the CDG fill is conducted as a parametric study in this study. The test cases are referred to as “High Permeability (HP)” cases. Additionally, in order to study the effect of previous rainfall and replicate the possible actual slope conditions that led to failures, a 19-day rainfall is applied to the slope prior to the “main rainfall event” as shown in Fig. 2. These cases will be referred as “With Previous Rainfall” (WP) cases. The summary of the test cases is shown in the table on the top right of Fig. 2. The bars located below Fig. 3d–f indicate the distribution of hourly rainfall intensity which are larger than 10, 20, and 30 mm/h.

Model validation

Using the numerical approach described in previous sections and summarized in Fig. 2, the rainfall events at Sau Mau Ping areas are simulated. The rainfall durations of the 1966, 1972, and 1976 events are 48, 50, and 34 h, respectively, corresponding to approximately 470 mm of total rainfall by the end of the calculation. In order to assist in the comparison of the slope performance under these rainfalls, we use calculation time to represent the results. The time $t = 1$ h represents the results at the end of the calculation after being subjected to 1-h rainfall from $t = 0$ h to $t = 1$ h.

Figure 5a–c and d–f summarizes the safety factors of SMP72 and SMP6, respectively, at different calculation times after being subjected to different rainfall events. The red, blue, and green lines represent the main analysis (MA), high permeability (HP), and with previous (WP) rainfall cases, respectively. The bar charts at the bottom of Fig. 5d–f denote the distribution of rainfall intensity greater than 10, 20, and 30 mm/h. The initial safety factors for MA and HP cases are identical as they have identical initial seepage conditions. The initial safety factors of SMP72 and SMP6 are 1.249 and 1.165, respectively. Likewise, with different initial conditions, all the WP cases have different initial safety factors, depending on the rainfall cases. As shown in Fig. 5, the slope stability, quantified by the safety factor, increases and decreases with calculation time, depending on the rainfall loadings. Table 2 summarizes all the initial and minimum safety factors. The value inside the brackets refers to the calculation time at which the minimum safety factor is reached.

The 1972 failure happened on June 18, 1972, at 1.24 p.m., corresponding to the calculation time between 49 and 50 h of the 1972 rainfall event. As shown in Fig. 5b, the safety factor of the WP case constantly decreases and reaches the $FOS_{\min} = 1.004$ at calculation time $t = 50$ h. Likewise, the 1976 failure occurred on August 25, 1976, at 10.12 a.m., approximately corresponding to $t = 34$ h. The safety factor of the WP case is equal to 1.004 at calculation time $t = 34$ h (Fig. 5f). Hence, both failure cases are properly replicated by the WP cases.

Additionally, according to the forensic report, the failure zone at Sau Mau Ping was generally confined within the top 3 m of the slope surface. Moreover, it was recorded that only a small portion of the stone pitching was removed in the 1976 failure. This means the failure zone was concentrated in the upper part of the slope. Figure 6

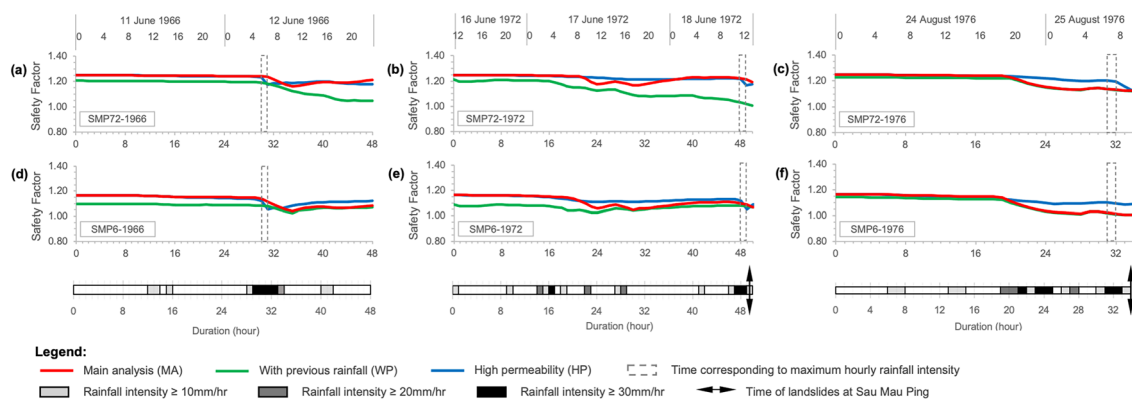


Fig. 5 Summary of changes in factor of safety (FOS) with respect to time and applied rainfall

Table 2 Summary of slope stability analysis results

Rainfall scenarios	SMP72						SMP6					
	Main analysis (MA)		With previous rainfall (WP)		High permeability (HP)		Main analysis (MA)		With previous rainfall (WP)		High permeability (HP)	
	Initial	Min.	Initial	Min.	Initial	Min.	Initial	Min.	Initial	Min.	Initial	Min.
1966	1.249	1.159 (35)	1.206	1.046 (47)	1.249	1.175 (31)	1.165	1.040 (35)	1.097	1.025 (35)	1.165	1.025 (35)
1972	1.249	1.166 (30)	1.212	1.004 (50)	1.249	1.167 (49)	1.165	1.046 (30)	1.087	1.023 (24)	1.165	1.049 (49)
1976	1.249	1.123 (34)	1.229	1.120 (34)	1.249	1.122 (34)	1.165	1.005 (34)	1.142	1.004 (34)	1.165	1.087 (33)

The calculation time at which the minimum safety factor is reached is shown in the brackets; the physical failure case is denoted in bold

displays the critical slip surface for the WP cases at the initial time (dotted red line) and when the minimum safety factor is reached (green areas). The initial depth of the slip surface is 1.5 m and 3 m for the SMP72-1972-WP and SMP6-1976-WP, respectively. After the 1972 rainfall, at $t = 50$ h, the SMP72's slip surface is located at the lower half of the slope with a depth of 2.2 m (Fig. 6a). Likewise, the slip surface of SMP6 after the 1976 rainfall ($t = 34$ h) is found to be concentrated at the upper half of the slope with a maximum depth of 1.3 m (Fig. 6b). Hence, the numerical results agree with the field investigation.

Results and discussion

Rainfall characteristics

Figure 3 summarizes all rainfall inputs used in this study. The “previous rainfall event” refers to the rainfall applied to the slope to simulate different initial conditions for WP cases. The 1966 “previous rainfalls” (Fig. 3a) tend to spread closer to the “main rainfall.” Four days before the “main rainfall,” the daily rainfall intensity is higher than 40 mm. The 1972 “previous rainfalls” (Fig. 3b) are relatively spread throughout the 19-day duration. However, to ensure the same cumulative rainfall intensity for the “main rainfall,” half of the rainfall intensity on 16/6/1972 is modeled as previous rainfall with rainfall intensity of approximately 100 mm/day. On the contrary, the 1976 “previous rainfalls” (Fig. 3c) are concentrated in the first half of the duration. The “main rainfall” is preceded by nine days without rainfall.

The 1966 “main rainfall” (Fig. 3d) resembles Rahimi et al.'s (2011) definition of a “normal” rainfall pattern with positive kurtosis as described by Fan et al. (2020). The bar chart at the bottom facilitates us in evaluating the distribution of rainfall intensity. Generally, high-intensity rainfalls are centered around $t = 28$ – 34 h with a maximum intensity of 108 mm/h at $t = 31$ h. The rainfall patterns in 1972 (Fig. 3e) are generally more scattered. As we can see from the bar chart at the bottom, several high-intensity rainfalls are scattered during the early duration of the rainfall. It is followed by 2 h of extreme rainfall intensity of 62 and 99 mm/h at $t = 48$ h and $t = 49$ h, respectively. It resembles a delayed high-intensity rainfall pattern. The 1976 rainfall (Fig. 3f) can be described as more compact. As shown from the bar chart at the bottom, the grey colors, representing rainfall intensity higher than 10 mm/h, are closer to each other. It resembles uniform distribution with slightly increasing intensity towards the end of the rainfall duration.

Slope stability

The slope SMP72 has a higher initial safety factor than the SMP6 for all MA, HP, and WP cases. This is probably attributed to the shape of the slope. As the SMP6 has a thicker loose fill layer and higher slope angle, it tends to be less stable in comparison to SMP72, thus the lower initial safety factor.

The less permeable layer of MDG/SDG bedrock introduces a semi-impermeable boundary to both slopes. The semi-impermeable boundary hinders the water from infiltrating the deeper layers of the slope. This behavior particularly affects the SMP72 slope as it has shallower fill layers. When the minimum FOS is reached, as shown in Fig. 6a, there is a significant amount of perched groundwater near the toe of SMP72. On the contrary, a lesser amount is

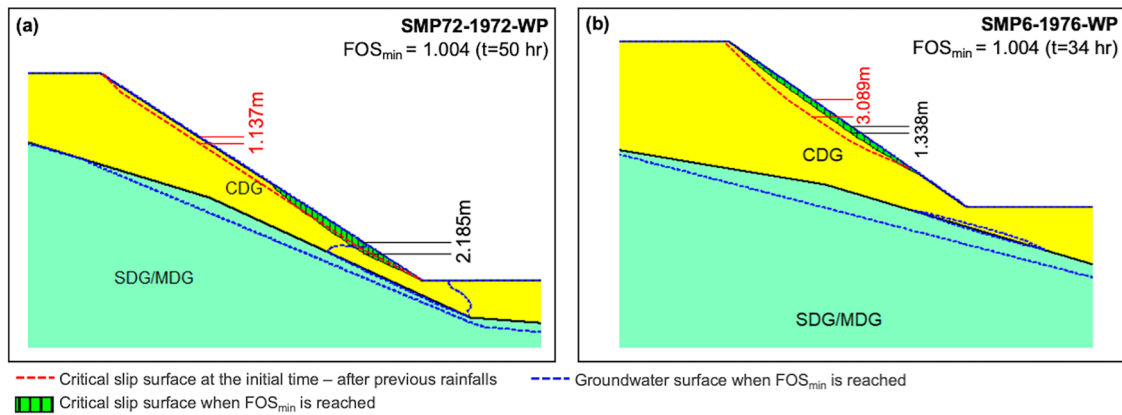


Fig. 6 Summary of slip surface at the time of minimum factor of safety (FOS) for **a** SMP72 and **b** SMP6 with considerations of previous rainfalls (WP)

observed on SMP6 (Fig. 6b). It is also interesting to note that the slopes with more permeable fill layers do not directly translate to lower stability. In the MA and HP cases, the initial seepage and stability conditions are identical for slopes with the same geological and hydrological settings. The HP cases of SMP72 have safety factors slightly lower than the MA cases. On the contrary, for SMP6, the HP cases relatively have a higher safety factor than MA cases. This is potentially due to the slope geometry, which in the case of SMP72, facilitates the formation of a perched water table. This highlights the role of the combined geological and hydrological settings as facilitating factors for rainfall-induced failure.

When comparing the MA cases, the 1976 rainfall results in the lowest safety factor for both SMP6 and SMP72 (Fig. 5c, f; Table 2). In fact, even without the influence of “previous rainfall,” the 1976 rainfall alone is able to cause SMP6 to fail; as shown in Table 2, the minimum safety factor of SMP6-1976-MA was 1.005 at $t = 34$ h. Despite the contradiction with the common assumption that the danger is related to high-intensity rainfall, it is generally consistent with the study of Fan et al. (2020), who concluded that relatively uniform rainfall leads to more water infiltration into the soil layer and subsequently introduces more substantial hazards compared to delayed high-intensity rainfall like the 1966 and 1972 events.

It is interesting to compare the MA and WP cases for the SMP72 under the 1972 rainfall. Despite having high rainfall intensity, the slope seems able to sustain the “main analysis” rainfall. The minimum safety factor of the MA case was not reached after the

high-intensity rain at $t = 50$ h, but at $t = 30$ h. However, when the “previous rainfall” is considered, as in the WP case, the SMP72 failed at $t = 50$ h, which agrees with the actual failure time. The possible explanation is discussed in the next section.

Seepage analysis

The role of rainfall pattern towards slope stability is closely associated with the amount of water infiltrated in or evaporated from the slope. A commonly adopted assumption is that the maximum rainwater that can infiltrate the soil equals the saturated permeability of the soil. Figure 7 shows that it might not always be the case, especially during the early calculation periods of MA cases or the periods after a certain duration without rainfall. Figure 8 shows that for these durations, the degree of saturation is close to one, but not yet fully saturated. Similar behavior has been observed by Gasmo et al. (2000), who utilized Darcy’s law—water flux is a function of permeability and head differences—to explain such behavior. The infiltration process is controlled by the infiltration capacity and pressure head differences rather than by the permeability itself. As highlighted in Fig. 7, despite having rainfalls of extreme intensity in 1966 and 1972, there exists a maximum amount of water infiltrating the soil. The 1966 rainfall, which has the highest hourly rainfall intensity, leads to the lowest cumulative infiltration compared to the 1972 and 1976 events. This shows that the rainfall intensity alone may not be a good predictor of the total

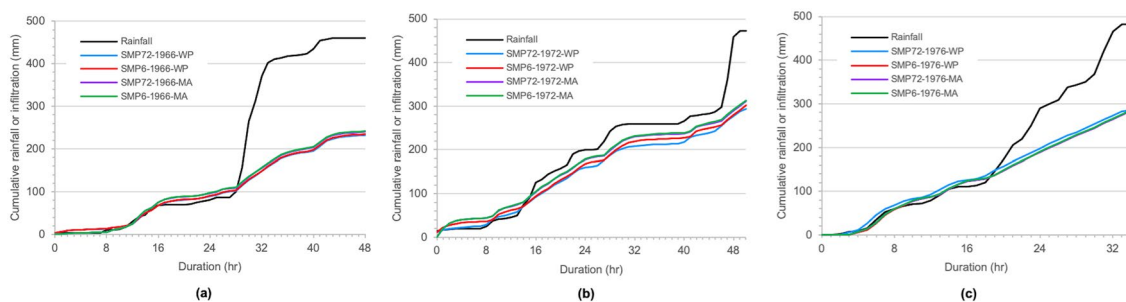


Fig. 7 Cumulative rainfall intensity and cumulative water infiltration under **a** 1966, **b** 1972, and **c** 1976 rainfall

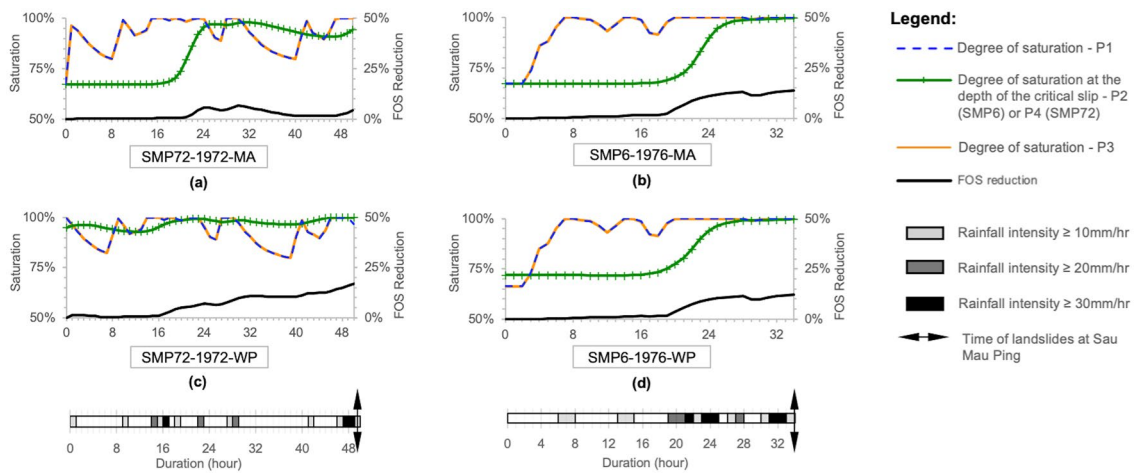


Fig. 8 Changes in degree of saturations at flux point P1, P2, P3, and P4 and reduction of factor of safety with time and applied rainfall

amount of rainwater infiltrating the slope. In reality, however, the excess rainfall should not be overlooked, as it can become runoff that might cause erosion. When erosion occurs, it might redistribute the slope's stress, which could also lead to slope failure (Cascini et al. 2010; Yang et al. 2021).

Equation 2 gives the relationship between the degree of saturation and soil strength. Likewise, Fig. 8 shows the relationship between the degree of saturation at the slip surface (green line) and the safety factor reduction (black line). The lines generally have the same trend, although with different magnitudes. This result suggests that slope stability is controlled by the degree of saturation of the soil mass within the slope, not only those on the surface. Additionally, by comparing the blue and orange lines with the bar chart at the bottom of the figures, the degree of saturation of the slope surface seems to be strongly affected by the rainfall pattern.

As previously mentioned, the MA and WP cases for SMP6 under the 1976 rainfall give almost an identical safety factor (Fig. 5f). Due to the 9-day no-rain period prior to the “main rainfall event,” the degree of saturation at the slope and slip surface only differ by a slight amount (Fig. 8b, d). The compacted pattern of the 1976 rainfall ensures that the slope is sufficiently saturated to facilitate water infiltrating deeper into the soil mass. A continuous reduction of the safety factor can be observed after calculation time $t = 19$ h, which leads to failure at $t = 34$ h for both MA and WP cases.

On the contrary, by comparing Fig. 8a, b, it can be observed that the influence of the previous rainfall events is substantial for the 1972 case. The degree of saturation at the slope's surface and slip surface is almost fully saturated after the “previous rainfall.” In both MA and WP cases, the FOS reduction can be observed after continuous rainfall at $t = 8$ – 32 h. However, the FOS increases in the MA case throughout the following 7-h no-rainfall period, while the FOS seems to be constant in the WP case (Figs. 5b and 8a, b). As a result, when the extreme rainfall intensity happened at $t = 48$ – 49 h, the WP case failed at a similar time recorded on the forensic report ($t = 50$ h). It should be noted, however, as shown in Fig. 5, the high-intensity rainfall is still related to the significant reduction of safety factors. The dotted grey lines in Fig. 5 correspond to the highest rainfall intensity, and most of the substantial reduction of the stability occurs during or not long after that.

When comparing the 1976 rainfall with the other, it seems that the variations of the degree of saturation at the slip surface, the safety factor reduction, and the cumulative infiltration caused by the 1966 and 1972 rainfalls generally occur in steps (Figs. 5, 7, and 8), which might be credited to the compacted nature of the 1976 rainfall that resembles a “uniform” distribution. Likewise, from the 1966 and 1972 rainfall, it can be concluded that when there is only rainfall of low intensity or no rainfall, the slope regains its suction strength and stability, although by slight amounts.

Figure 9 summarizes the pore water pressure profile at cross-sections S1 and S2 for SMP72 under 1972 rainfall and for SMP6 under 1976 rainfall. The general behavior agrees with previous studies (Collins and Znidarcic 2004; Lu and Godt 2008; Godt et al. 2012). As the rainfall event commences, the suction will gradually reduce, and the wetting front will be developed deeper. The contribution of previous rainfall towards initial seepage conditions can be observed by comparing MA and WP cases in Figs. 8 and 9. The previous rainfall is shown to infiltrate further to the slope, facilitating a deeper wetting front (Fig. 9). In the case of SMP72 (Fig. 9d), it further facilitates the formation of perched groundwater. From all test cases, there is no significant change in the initial groundwater table. This finding agrees with the previous observation that only 2% of slope failures in Hong Kong were attributed to the rise of groundwater level (Wong and Ho 1993). There is an interesting observation between $t = 32$ – 40 h for the SMP72 (Fig. 9a–d) cases: as the rainfall intensity occurring at that duration is low, the upper portion of the suction seems to regain slowly before it diminishes under the afterward high-intensity rainfall ($t = 48$ – 50 h). A similar observation can also be seen in the pore water pressure after the previous rainfall events for SMP6 (Fig. 9e, h). Again, this observation highlights the effect of the temporal pattern of antecedent rainfalls; in this case, the absence of rainfall between the events allows the suction strength to regain in the slope.

Limitations and future study

It is a challenge to accurately estimate the actual infiltration rate for a hillslope as it involves complex interplays of different factors. All

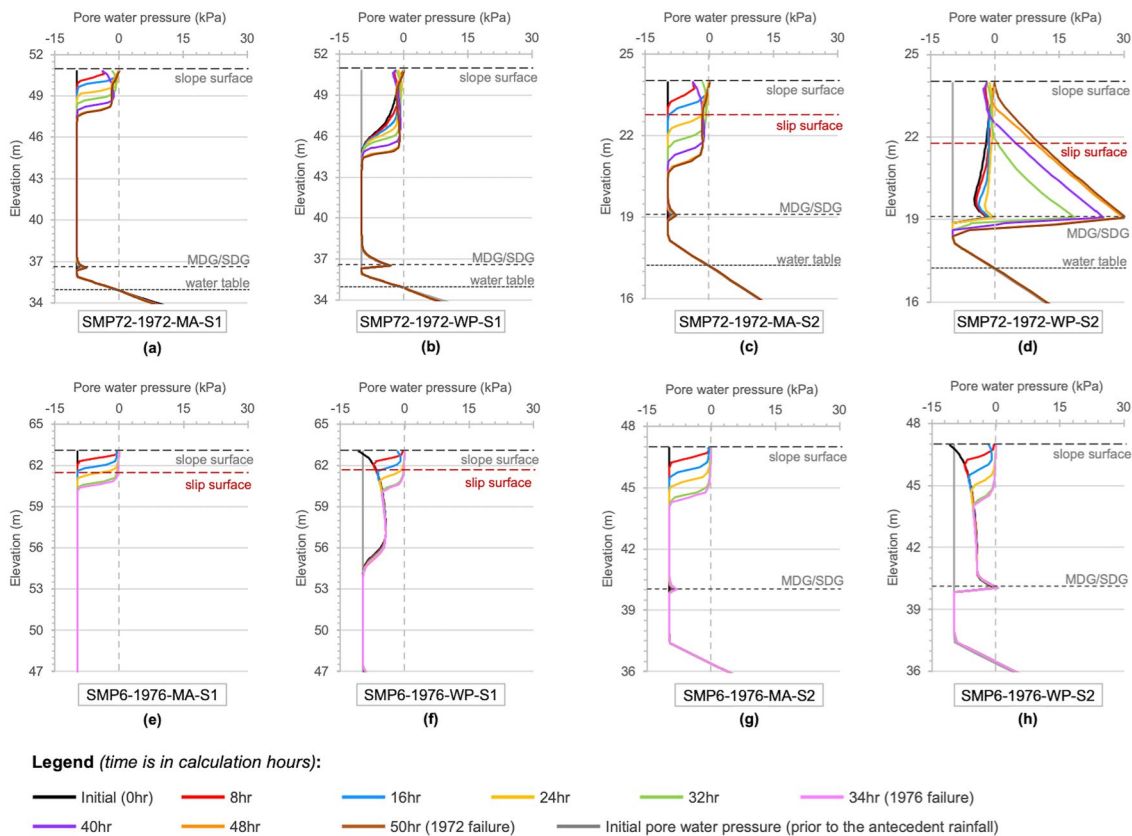


Fig. 9 Pore water pressure profile at the cross-section S1 (near crest) and S2 (near toe) at **a–d** SMP72 and **e–h** SMP6

the rainfall intensities are based on “clock hours” and are unlikely to represent the maximum hourly rainfall amounts or the true distributions of the intensities. Binnie and Partners (1976) averaged the rain gauge measurements from all nearby gauges and presented the possibility that the actual rainfall occurring on site was less severe in 1966 and 1972 compared to 1976. Despite this uncertainty, our study has shown that even with lower maximum rainfall intensity, the more compacted and uniform rainfall temporal pattern in 1976 could lead to more water infiltration and almost no chance for the soil strength and slope stability to regain in between the rainfalls, thus leading to the devastating failure of the slopes which had previously survived the previous extreme rainfalls. Additionally, field measurements have reported the presence of substantial variabilities within the slopes in Sau Mau Ping. Future studies to evaluate how these uncertainties and variabilities affect slope stability regarding its response to rainfall patterns and antecedent conditions would be worthwhile.

Another possible failure mechanism for loose fill slopes under rainfall is the instability under the constant shear drained (CSD) stress path (Anderson and Sitar 1995; Cascini et al. 2010; Dong et al. 2016). Most recent attempts in this regard include that by Chen and Yang (2023) and Zhang et al (2023), who examined the correspondence between soil responses under the CSD stress path and the undrained triaxial compression path. While the CSD response can be reproduced in laboratory element tests and in element simulations for saturated soils, it remains uncertain whether it can occur

in physical model tests (Take et al. 2004) or in field conditions for which soils are largely unsaturated. As far as numerical modeling of this failure mechanism in real slopes is concerned, it requires fully coupled, nonlinear finite element analyses and sophisticated soil models. Future work in this regard would be worthwhile. Nevertheless, the great uncertainty in determining many parameters involved in advanced soil models and the numerical difficulty in coupled nonlinear computation cannot be overlooked.

Summary and conclusions

Rainfall-induced slope failures can pose a massive danger to our natural and built environment. Despite numerous studies over the past decades, it remains a big challenge to properly predict and prevent large landslides associated with heavy rainfalls. In this study, an effort has been made to study the role of rainfall temporal patterns and successfully apply it to address an intriguing question in relation to the catastrophic landslides at Sau Mau Ping, Hong Kong, in 1972 and 1976: why did the slopes that withstood the 1972 rainfall fail in the 1976 rainfall, given that the intensity of the latter was only half of the former? The case references have been revisited by integrating the geological, hydrological, and climatological aspects and by a combination of seepage and stability modeling. The main results and findings of this study are summarized as follows.

- (a) The long duration and relatively uniform rainfall temporal pattern, like the August 1976 rainfall event, can pose greater

danger than the delayed high-intensity rainfall. This explains why the slopes that previously survived the 1972 rainfall failed in 1976

- (b) The 1972 failure event was caused by a devastating combination of antecedent conditions and extreme rainfall facilitated by the geological and hydrological settings of SMP72 slope. The combination of shallow bedrock and rainfall with a delayed-high-intensity temporal pattern facilitated the development of a perched water table that could exacerbate the failure
- (c) The analysis of the 1976 failure suggests that focusing only on cumulative rainfall intensity, duration, and frequency in developing threshold conditions to predict rainfall-induced slope failures, without considering the temporal pattern of the antecedent and main rainfall, may be unconservative
- (d) Unlike the commonly used assumption, the rainwater infiltration rate can be larger than the saturated permeability of the soil. Therefore, using this assumption in the future analysis should proceed with caution
- (e) The increase in groundwater level due to rainfall is generally limited. Therefore, its contribution towards slope failure depends on the geological and hydrological settings of the slope
- (f) The presence of low intensity or no rain period contributes to the magnitude of the suction in the slope and thus contributes to slope stability

Funding

The financial support provided by the Research Grants Council of Hong Kong through the GRF Grant No. 17207923 and the HKPF scheme is gratefully acknowledged.

Data availability

All data supporting the findings in this article are available from the corresponding author upon reasonable request.

Declarations

Competing interests The authors declare no competing interests.

Open Access This article is licensed under a Creative Commons Attribution 4.0 International License, which permits use, sharing, adaptation, distribution and reproduction in any medium or format, as long as you give appropriate credit to the original author(s) and the source, provide a link to the Creative Commons licence, and indicate if changes were made. The images or other third party material in this article are included in the article's Creative Commons licence, unless indicated otherwise in a credit line to the material. If material is not included in the article's Creative Commons licence and your intended use is not permitted by statutory regulation or exceeds the permitted use, you will need to obtain permission directly from the copyright holder. To view a copy of this licence, visit <http://creativecommons.org/licenses/by/4.0/>.

References

- Anderson SA, Sitar N (1995) Analysis of rainfall-induced debris flows. *J Geotechnical Eng* 121:544–552. [https://doi.org/10.1061/\(asce\)0733-9410\(1995\)121:7\(544\)](https://doi.org/10.1061/(asce)0733-9410(1995)121:7(544))
- Binnie, Partners (1976) Report on the slope failures at Sau Mau Ping 25th August 1976 Volume 1–3
- Cascini L, Cuomo S, Pastor M, Sacco C (2013) Modelling the post-failure stage of rainfall-induced landslides of the flow type. *Can Geotech J* 50:924–934. <https://doi.org/10.1139/cgj-2012-0375>
- Cascini L, Cuomo S, Pastor M, Sorbino G (2010) Modeling of rainfall-induced shallow landslides of the flow-type. *J Geotech Geoenviron* 136:85–98. [https://doi.org/10.1061/\(asce\)gt.1943-5606.0000182](https://doi.org/10.1061/(asce)gt.1943-5606.0000182)
- Chen C-W, Oguchi T, Hayakawa YS et al (2017) Relationship between landslide size and rainfall conditions in Taiwan. *Landslides* 14:1235–1240. <https://doi.org/10.1007/s10346-016-0790-7>
- Chen Y, Yang J (2023) Initiation of flow liquefaction in granular soil slopes: drained versus undrained conditions. *Acta Geotechnica*. <https://link.springer.com/article/10.1007/s11440-023-01958-6>
- Chitu Z, Bogaard T, Busuioc A et al (2017) Identifying hydrological pre-conditions and rainfall triggers of slope failures at catchment scale for 2014 storm events in the Ialomita Subcarpathians, Romania. *Landslides* 14:419–434. <https://doi.org/10.1007/s10346-016-0740-4>
- Chiu CF, Yan WM, Yuen K-V (2012) Reliability analysis of soil–water characteristics curve and its application to slope stability analysis. *Eng Geol* 135:83–91. <https://doi.org/10.1016/j.enggeo.2012.03.004>
- Collins BD, Znidarcic D (2004) Stability analyses of rainfall induced landslides. *J Geotech Geoenviron* 130:362–372. [https://doi.org/10.1061/\(asce\)1090-0241\(2004\)130:4\(362\)](https://doi.org/10.1061/(asce)1090-0241(2004)130:4(362))
- Dong Q, Xu C, Cai Y et al (2016) Drained instability in loose granular material. *Int J Geomech* 16:04015043. [https://doi.org/10.1061/\(asce\)gm.1943-5622.0000524](https://doi.org/10.1061/(asce)gm.1943-5622.0000524)
- Eckersley D (1990) Instrumented laboratory flowslides. *Géotechnique* 40:489–502. <https://doi.org/10.1680/geot.1990.40.3.489>
- Fan L, Lehmann P, Zheng C, Or D (2020) Rainfall intensity temporal patterns affect shallow landslide triggering and hazard evolution. *Geophys Res Lett*. <https://doi.org/10.1029/2019gl085994>
- Fredlund DG, Xing A (1994) Equations for the soil–water characteristic curve. *Can Geotech J* 31:521–532. <https://doi.org/10.1139/t94-061>
- Fredlund DG, Xing A, Huang S (1994) Predicting the permeability function for unsaturated soils using the soil–water characteristic curve. *Can Geotech J* 31:533–546. <https://doi.org/10.1139/t94-062>
- Fredlund DG, Rahardjo H, Fredlund MD (2012) Unsaturated soil mechanics in engineering practice. Wiley, Hoboken, USA
- Gao L, Zhang LM, Cheung RWM (2018) Relationships between natural terrain landslide magnitudes and triggering rainfall based on a large landslide inventory in Hong Kong. *Landslides* 15:727–740. <https://doi.org/10.1007/s10346-017-0904-x>
- Gasmo JM, Rahardjo H, Leong EC (2000) Infiltration effects on stability of a residual soil slope. *Comput Geotech* 26:145–165. [https://doi.org/10.1016/s0266-352x\(99\)00035-x](https://doi.org/10.1016/s0266-352x(99)00035-x)
- GeoSlope, (2018) Users manual. Geo-Slope International Ltd., Calgary, Canada
- Godt JW, Baum RL, Lu N (2009) Landsliding in partially saturated materials. *Geophys Res Lett*. <https://doi.org/10.1029/2008gl035996>
- Godt JW, Şener-Kaya B, Lu N, Baum RL (2012) Stability of infinite slopes under transient partially saturated seepage conditions. *Water Resour Res*. <https://doi.org/10.1029/2011wr011408>
- Guzzetti F, Peruccacci S, Rossi M, Stark CP (2007) Rainfall thresholds for the initiation of landslides in central and southern Europe. *Meteorol Atmos Phys* 98:239–267. <https://doi.org/10.1007/s00703-007-0262-7>
- Guzzetti F, Peruccacci S, Rossi M, Stark CP (2008) The rainfall intensity–duration control of shallow landslides and debris flows: an update. *Landslides* 5:3–17. <https://doi.org/10.1007/s10346-007-0112-1>
- Harilal GT, Madhu D, Ramesh MV, Pullarkatt D (2019) Towards establishing rainfall thresholds for a real-time landslide early warning system in Sikkim, India. *Landslides* 16:2395–2408. <https://doi.org/10.1007/s10346-019-01244-1>
- HKIE (2003) Soil nails in loose fill slopes - a preliminary study. The Geotechnical Division of Hong Kong Institution of Engineers

- Hong M, Kim J, Jeong S (2018) Rainfall intensity-duration thresholds for landslide prediction in South Korea by considering the effects of antecedent rainfall. *Landslides* 15:523–534. <https://doi.org/10.1007/s10346-017-0892-x>
- Hong Kong Observatory (2023) Daily extract of meteorological observations. <https://www.hko.gov.hk/en/cis/dailyExtract.htm?y=1972&m=6>. Accessed 7 Jul 2022
- Ibsen M-L, Casagli N (2004) Rainfall patterns and related landslide incidence in the Porretta-Vergato region, Italy. *Landslides* 1:143–150. <https://doi.org/10.1007/s10346-004-0018-0>
- Iverson RM (2000) Landslide triggering by rain infiltration. *Water Resour Res* 36:1897–1910. <https://doi.org/10.1029/2000wr900090>
- Jiao JJ, Wang X-S, Nandy S (2005) Confined groundwater zone and slope instability in weathered igneous rocks in Hong Kong. *Eng Geol* 80:71–92. <https://doi.org/10.1016/j.enggeo.2005.04.002>
- Johnson KA, Sitar N (1990) Hydrologic conditions leading to debris-flow initiation. *Can Geotech J* 27:789–801. <https://doi.org/10.1139/t90-092>
- Johnston EC, Davenport FV, Wang L et al (2021) Quantifying the effect of precipitation on landslide hazard in urbanized and non-urbanized areas. *Geophys Res Lett*. <https://doi.org/10.1029/2021gl094038>
- Jones JN, Boulton SJ, Bennett GL et al (2021) Temporal variations in landslide distributions following extreme events: implications for landslide susceptibility modeling. *J Geophys Res Earth Surf*. <https://doi.org/10.1029/2021jg006067>
- Kim SW, Chun KW, Kim M et al (2021) Effect of antecedent rainfall conditions and their variations on shallow landslide-triggering rainfall thresholds in South Korea. *Landslides* 18:569–582. <https://doi.org/10.1007/s10346-020-01505-4>
- Knill JL, Lumb P, Mackey S et al (1999) Report of the independent review panel on fill slopes. GEO Report No. 86, Geotechnical Engineering Office, Hong Kong Special Administrative Region
- Kong VWW, Kwan JSH, Pun WK (2020) Hong Kong's landslip warning system—40 years of progress. *Landslides* 17:1453–1463. <https://doi.org/10.1007/s10346-020-01379-6>
- Lee J-H, Kim H, Park H-J, Heo J-H (2021) Temporal prediction modeling for rainfall-induced shallow landslide hazards using extreme value distribution. *Landslides* 18:321–338. <https://doi.org/10.1007/s10346-020-01502-7>
- Li A (2003) Field monitoring of a saprolite cut slope. PhD thesis, The University of Hong Kong, Hong Kong
- Li AG, Yue ZQ, Tham LG et al (2005) Field-monitored variations of soil moisture and matric suction in a saprolite slope. *Can Geotech J* 42:13–26. <https://doi.org/10.1139/t04-069>
- Lu N, Godt J (2008) Infinite slope stability under steady unsaturated seepage conditions. *Water Resour Res*. <https://doi.org/10.1029/2008wr006976>
- Luo HY, Zhang LM, Wang HJ, He J (2021) Process of building collapse caused by the Po Shan Road landslide in Hong Kong on 18 June 1972. *Landslides* 18:3769–3780. <https://doi.org/10.1007/s10346-021-01745-y>
- Malone AW (1988) The role of government in landslide disaster prevention in Hong Kong and Indonesia. *Geotech Eng* 19:227–252
- Mathew J, Babu DG, Kundu S et al (2014) Integrating intensity–duration-based rainfall threshold and antecedent rainfall-based probability estimate towards generating early warning for rainfall-induced landslides in parts of the Garhwal Himalaya, India. *Landslides* 11:575–588. <https://doi.org/10.1007/s10346-013-0408-2>
- Napolitano E, Fusco F, Baum RL et al (2016) Effect of antecedent-hydrological conditions on rainfall triggering of debris flows in ash-fall pyroclastic mantled slopes of Campania (southern Italy). *Landslides* 13:967–983. <https://doi.org/10.1007/s10346-015-0647-5>
- Natalia L, Yang J (2022) Investigation of rainfall-induced slope failures from an integrated perspective. In: Cloutier C, Turmel D, Maghoul P, Locat A (eds) 8th Canadian Conference on Geotechnique and Natural Hazards. pp 457–463
- Ng CWW (2008) Deformation and failure mechanisms of loose and dense fill slopes with and without soil nails. *Proc of 10th Int Sym on Landslides and Engineered Slopes*. Xi'an, China 1:159–177
- Ng CWW, Crous PA, Zhang M, Shakeel M (2022) Static liquefaction mechanisms in loose sand fill slopes. *Comput Geotech* 141:104525. <https://doi.org/10.1016/j.compgeo.2021.104525>
- Ng CWW, Fung WT, Cheuk CY, Zhang L (2004) Influence of stress ratio and stress path on behavior of loose decomposed granite. *J Geotech Geoenviron* 130:36–44. [https://doi.org/10.1061/\(asce\)1090-0241\(2004\)130:1\(36\)](https://doi.org/10.1061/(asce)1090-0241(2004)130:1(36))
- Parsons AJ, Stone PM (2006) Effects of intra-storm variations in rainfall intensity on interrill runoff and erosion. *CATENA* 67:68–78. <https://doi.org/10.1016/j.catena.2006.03.002>
- Royal Observatory (1977) Meteorological results 1976: part III - tropical cyclone summaries. Government Printer, Hong Kong
- Royal Observatory (1979) Technical note no. 51: the severe rainfall occasion, 16–18 June 1972. Royal Observatory, Hong Kong
- Rahardjo H, Ong TH, Rezaur RB, Leong EC (2007) Factors controlling instability of homogeneous soil slopes under rainfall. *J Geotech Geoenviron* 133:1532–1543. [https://doi.org/10.1061/\(asce\)1090-0241\(2007\)133:12\(1532\)](https://doi.org/10.1061/(asce)1090-0241(2007)133:12(1532))
- Rahardjo H, Leong EC, Rezaur RB (2008) Effect of antecedent rainfall on pore-water pressure distribution characteristics in residual soil slopes under tropical rainfall. *Hydrol Process* 22:506–523. <https://doi.org/10.1002/hyp.6880>
- Rahimi A, Rahardjo H, Leong E-C (2011) Effect of antecedent rainfall patterns on rainfall-induced slope failure. *J Geotech Geoenviron* 137:483–491. [https://doi.org/10.1061/\(asce\)gt.1943-5606.0000451](https://doi.org/10.1061/(asce)gt.1943-5606.0000451)
- Smolíkóvá J, Blahut J, Vilímek V (2016) Analysis of rainfall preceding debris flows on the Smědavská hora Mt., Jizerské hory Mts. Czech Republic *Landslides* 13:683–696. <https://doi.org/10.1007/s10346-015-0601-6>
- Springman SM, Thielen A, Kienzler P, Friedel S (2013) A long-term field study for the investigation of rainfall-induced landslides. *Géotechnique* 63:1177–1193. <https://doi.org/10.1680/geot.11.p.142>
- Sun HW (1999) Review of fill slope failures in Hong Kong. GEO Report No. 96, Geotechnical Engineering Office, Hong Kong Special Administrative Region
- Sweeney DJ, Robertson PK (1979) A fundamental approach to slope stability problems in Hong Kong. *Hong Kong Engineer* 7(10):35–44
- Take WA, Beddoe RA, Davoodi-Bilesavar R, Phillips R (2015) Effect of antecedent groundwater conditions on the triggering of static liquefaction landslides. *Landslides* 12:469–479. <https://doi.org/10.1007/s10346-014-0496-7>
- Take WA, Bolton MD, Wong PCP, Yeung FJ (2004) Evaluation of landslide triggering mechanisms in model fill slopes. *Landslides* 1:173–184. <https://doi.org/10.1007/s10346-004-0025-1>
- Vail AJ (1984) Two landslides in Hong Kong. In: Proceedings of 4th international symposium on landslides. Toronto, Canada
- Vanapalli SK, Fredlund DG, Pufahl DE, Clifton AW (1996) Model for the prediction of shear strength with respect to soil suction. *Can Geotech J* 33:379–392. <https://doi.org/10.1139/t96-060>
- Wang G, Sassa K (2001) Factors affecting rainfall-induced flowslides in laboratory flume tests. *Géotechnique* 51:587–599. <https://doi.org/10.1680/geot.2001.51.7.587>
- Wang G, Sassa K (2003) Pore-pressure generation and movement of rainfall-induced landslides: effects of grain size and fine-particle content. *Eng Geol* 69:109–125. [https://doi.org/10.1016/s0013-7952\(02\)00268-5](https://doi.org/10.1016/s0013-7952(02)00268-5)
- Wong HN, Ho KKS (1993) Systematic investigation of landslides caused by a severe rainstorm in Hong Kong. *Hkie Transactions* 3:17–27. <https://doi.org/10.1080/1023697x.1996.10667704>
- Yang J (2002) Non-uniqueness of flow liquefaction line for loose sand. *Géotechnique* 54:66–68
- Yang J, Liang LB, Chen Y (2021) Instability and liquefaction flow slide of granular soils: the role of initial shear stress. *Acta Geotech*. <https://doi.org/10.1007/s11440-021-01200-1>
- Yang J, Wei LM (2012) Collapse of loose sand with the addition of fines: the role of particle shape. *Géotechnique* 62:1111–1125. <https://doi.org/10.1680/geot.11.p.062>
- Yang TL, Mackey S, Cumine E (1972) Interim report of the commission of inquiry into the rainstorm disasters 1972. Government Printer, Hong Kong

- Yang TL, Mackey S, Cumine E (2008) Final report of the commission of inquiry into the rainstorm disasters 1972. GEO Report No.229, Geotechnical Engineering Office, Hong Kong Special Administrative Region
- Yang S-Y, Jan C-D, Wang J-S (2018) Landslides triggered by Typhoon Morakot in Taiwan. *Environmental Risks*. <https://doi.org/10.5772/intechopen.76930>
- Yubonchit S, Chinkulkijniwat A, Horpibulsuk S et al (2017) Influence factors involving rainfall-induced shallow slope failure: numerical study. *Int J Geomech* 17:04016158. [https://doi.org/10.1061/\(asce\)gm.1943-5622.0000865](https://doi.org/10.1061/(asce)gm.1943-5622.0000865)
- Zhang L, Li J, Li X et al (2016) Rainfall-induced soil slope failure stability analysis and probabilistic assessment. CRC Press, Boca Raton
- Zhang L, Tang X, Yang J (2023) Rainfall-induced flowslides of granular soil slopes: insights from grain-scale modeling. *Eng Geol* 323:107223. <https://doi.org/10.1016/j.enggeo.2023.107223>
- Zhang L, Zhang J, Zhang LM, Tang WH (2011) Stability analysis of rainfall-induced slope failure: a review. *Proc Institution Civ Eng - Geotechnical Eng* 164:299–316. <https://doi.org/10.1680/geng.2011.164.5.299>
- Zhao Y, Meng X, Qi T et al (2022) Extracting more features from rainfall data to analyze the conditions triggering debris flows. *Landslides* 19:2091–2099. <https://doi.org/10.1007/s10346-022-01893-9>
-
- Levinna Natalia · Jun Yang** (✉)
Department of Civil Engineering, The University of Hong Kong,
Hong Kong, China
Email: junyang@hku.hk
-